ELSEVIER

Research article

Synthesis, crystal structures and electrochemical properties of ferrocenyl imidazole derivatives

Check for updates

Ayomide H. Labulo, Bernard Omondi, Vincent O. Nyamori [*]

School of Chemistry and Physics, University of KwaZulu-Natal, Westville Campus, Private Bag X54001, Durban, South Africa

ABSTRACT

Six ferrocenyl imidazole derivatives substituted with -Cl, -NO_2 and -CH_3 on the 2-position of the 1H-imidazole ring have been synthesized. Of the six compounds, the di-substituted ferrocenes, i.e. compounds **4** (1,1′-ferrocenylmethyl(2-chloroimidazole)), **5** (1,1′-ferrocenyl(2-nitroimidazole)), and **6** (1,1′-ferrocenylmethyl(2-methylimidazole)) are reported for the first time. The structure-property relationships of compounds **4**, **5** and **6** were investigated by means of UV-visible, FTIR, ¹H-NMR, ¹³C-NMR spectroscopy and electrochemical studies. UV-visible analysis in acetonitrile showed that the π -π* band of compounds **2** (1-ferrocenylmethyl(2-nitroimidazole)) and **5** appeared at longer wavelength compared to **1** (1-ferrocenylmethyl(2-chloroimidazole)), **3** (1-ferrocenylmethyl(2-methylimidazole)), **4** and **6**. This phenomenon is due to the different electronics around the imidazole moieties. In cyclic voltammetry analysis, all compounds exhibited a quasi-reversible redox wave for the ferrocenyl and imidazole moieties. Density functional theoretical (DFT) calculations with the B3LYP/6-311+G(d) basis set were performed on compounds **1**–**6**, and the calculated HUMO-LUMO band gap energies correlated with those obtained from electrochemical and spectroscopic data. The X-ray crystallographic analysis highlighted the effect of electron-withdrawing and electron-donating substituents on the conformation of the cyclopentadienyl rings attached to the ferrocenyl moiety.

1. Introduction

Ferrocenyl derivatives bearing heteroatoms, such as N, P and S, have been of great importance in organometallic chemistry. The synthesis of compounds containing the ferrocenyl unit with various acceptor units such as pyrrole [1], indole [2], thiourea [3], pyridine [4] and imidazole [5] have been previously reported. These particular ferrocenyl derivatives have potential applications in fields such as electrochemistry [6], medicinal science [7], nonlinear optics [8] and materials science [9, 10]. Ferrocenyl alkyl azoles have received considerable attention as a result of the unusual properties of the ferrocene system, and this is due to its unique steric protection, electron-donation properties and chemical stability [11]. The design and fabrication of series of donor-acceptor systems are increasing due to their use in the preparation of optoelectronics [12], liquid crystals [13], polymers [14], sensors [15] and magnetic materials [16]. The photonic and electronic properties of the donor-acceptor system can be fine-tuned by varying the acceptor, donor or spacer strength [17].

Several synthetic approaches have been exploited for the synthesis of ferrocenylalkyl azoles. Mono- and di-substituted ferrocenyl compounds

with *N*-heterocyclic groups, such as ferrocenylmethylbenzimidazole, have been reported [18]. Ferrocenylmethyl benzimidazole has been prepared according to the classical method, i.e. from the reaction of thionyldibenzimidazole and ferrocenylmethanol in dichloromethane [19]. 1-Ferrocenylethyl benzotriazole has also been synthesized by using 1-ferrocenylethanol and benzotriazole in dichloromethane in the presence of aqueous fluoroboric acid at room temperature [20]. An alternative approach for the synthesis of ferrocenylalkyl imidazoles has been proposed with the use of *N,N′*-carbonyldiimidazole (CDI) [16]. For example, 1,1′-bis(imidazolylmethyl)ferrocenes have been synthesized by the reaction of diferrocenemethanol with CDI [21] or phosphorous tribromide [5]. Simenel *et al.* [22] reported a simple method for the synthesis of ferrocenyl(alkyl)imidazoles. This method involves the treatment of ferrocenylcarbinols with CDI in methylene dichloride. Additionally, *N, N′*-diferrocenylimidazol(in)ium salts have been synthesized by condensation of *N,N′*-diferrocenyldiazabutadiene with formaldehyde [23]. The electrochemical behaviour of a range of ferrocenylalkyl azoles has been studied and the compounds were found to have low reduction potentials [24, 25]. The oxidation potentials (E_{pa}) for substituted ferrocenylalkyl azoles have been found to be markedly dependent on the degree of

---

* Corresponding author.
  E-mail address: nyamori@ukzn.ac.za (V.O. Nyamori).

electron-accepting or electron-donating properties of the lateral substituents [26].

In terms of applications, a number of ferrocenyl imidazole salt derivatives ferrocenyl imidazole salts, have been utilized in various applications. For example, ferrocenylalkyl imidazole salts have been found to play a vital role in many biological systems such as metallo-proteins [27] and anticancer drugs [18]. Ferrocenyl compounds connected to an imidazole ring, such as ferrocenylethyl-N'-(trimethylphenyl)imidazole chloride have been found to show antimicrobial activity [28]. Substituted ferrocenyl imidazoles have also been employed as the catalyst for the synthesis of nitrogen-doped carbon nanotubes (N-CNTs) and N-CNT-metal nanocomposites [11, 29]. These compounds have produced carbon nanomaterials with improved thermal [30, 31], structural [32] and magnetic [33] properties.

In this study, we report the synthesis and characterization of -Cl, -NO$_2$ and -CH$_3$ substituted ferrocenyl imidazole compounds. The synthesis of 1-ferrocenylmethyl(2-chloroimidazole) (1), 1-ferrocenylmethyl(2-nitroimidazole) (2) and 1-ferrocenylmethyl(2-methylimidazole) (3) have been reported in our previous work [29], however, the synthesis of 1,1′-ferrocenylmethyl(2-chloroimidazole) (4), 1,1′-ferrocenyl(2-nitroimidazole) (5) and 1,1′-ferrocenylmethyl(2-methylimidazole) (6) are reported for the first time. The structure-property relationships of compounds 1–6 were investigated. The redox behaviour and electronic transitions of compounds 1–6 were investigated by both experimental (cyclic voltammetry and UV-visible spectroscopy, respectively) and theoretical (density functional theory (DFT) calculations) studies. The molecular structures of compounds 4 and 5 were determined by X-ray crystallography.

2. Results and discussion

2.1. Synthesis and characterization

Mono- (1–3) and di-substituted (4–6) ferrocenyl imidazole compounds were synthesized following a literature method, i.e. the reaction of ferrocenemethanol and 1,1′-ferrocenedimethanol, respectively, with 2-substituted (-Cl, -NO$_2$ and -CH$_3$) 1H-imidazoles in the presence of glacial acetic acid [34] (Scheme 1). Compound 4 is an orange solid, while compounds 5 and 6 are high melting compounds obtained as yellow solids. All compounds were obtained in relatively high isolated yields (75–83%), similar to those reported in the synthesis of ferrocenyl alkyl imidazole compounds, obtained from the reaction of ferrocenemethanol

[35] and 1,1′-ferrocenedimethanol [5]. From ^{1}H-NMR spectra, characteristic resonances for imidazole protons appeared at 6.77–7.66 ppm and at 124.87–132.43 ppm for C5/C6 in the case of ^{13}C-NMR spectra (Table 1, Figs. 1 and 2). These values are similar to those reported for ferrocenyl(methyl)imidazole [36].

The resonance peaks of the unsubstituted ferrocenes and the substituted ferrocenes occur as a singlet between 4.12-4.23 ppm and as a triplet between 4.22-4.27 ppm, respectively [37]. The peak for C3-H was observed to be more downfield, i.e. 5.34 ppm for 2 and 5.38 ppm for 5, and this due to the electron-withdrawing inductive effect from the -NO$_2$ substituent (Fig. 1 and Scheme 1).

The appearance of a FTIR absorption band between 1248-1360 cm^{-1} was observed in all compounds. This peak marked the appearance of the C-N absorption band while the O-H bands of the starting ferrcocenyl alcohols disappeared. The most important frequencies for the ferrocene moiety are found at 450–481 (ν_{Fe-Cp}), 821–831 (πC–H), 1440 cm^{-1} (ν_{C-C}) and 3382-3113 cm^{-1} (ν_{C-H}) [37].

2.2. Crystal structures

Crystals of compounds 4 and 5 were grown in a dichloromethane-hexane solution. *ORTEP* drawings of these compounds together with the atom numbering schemes, are shown in Fig. 3. Selected bond angles and bond lengths for compounds 4 and 5 are listed in Table 2. The asymmetric unit of compound 4 contains one molecule while for compound 5 it contains half a molecule with the other half generated by the inversion centre on the Fe atom. The Cp rings in compound 5 adopt a perfect *anti*-conformation with a staggering angle of 35.82(4)°. In

Table 1
^{1}H-/^{13}C-NMR characteristic data for the imidazole moiety of compounds 1–6.

Compound	^{1}H-NMR (ppm)		^{13}C-NMR (ppm)		
	C3-H	C5/C6-H	C3	C4	C5/C6
1*	4.75	6.78/6.81	81.81	120.65	127.93/131.22
2*	5.34	6.92/7.01	80.15	144.47	124.87/128.04
3*	4.73	6.76/6.84	82.78	143.94	128.70/130.87
4	4.76	6.85/6.89	82.87	131.22	128.15/130.87
5	5.38	7.15/7.66	81.57	124.97	128.23/128.25
6	4.76	6.77/6.82	83.66	143.92	128.79/132.46

* Values taken from ref [29].
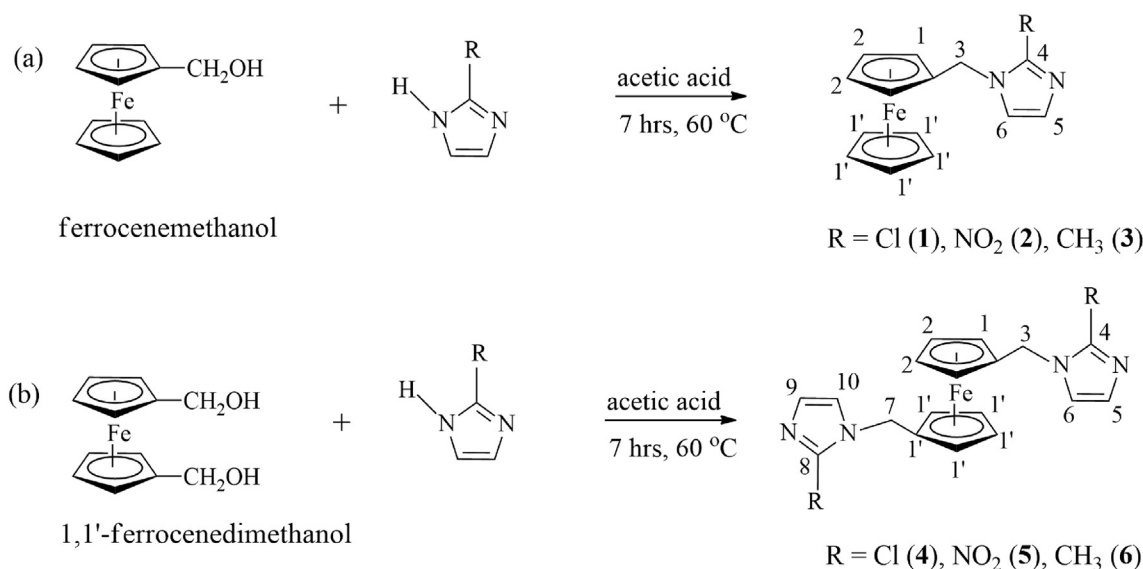
Scheme 1. Reaction schemes of (a) ferrocenemethanol and (b) 1,1′-diferrocenemethanol for the synthesis of compounds 1–6.
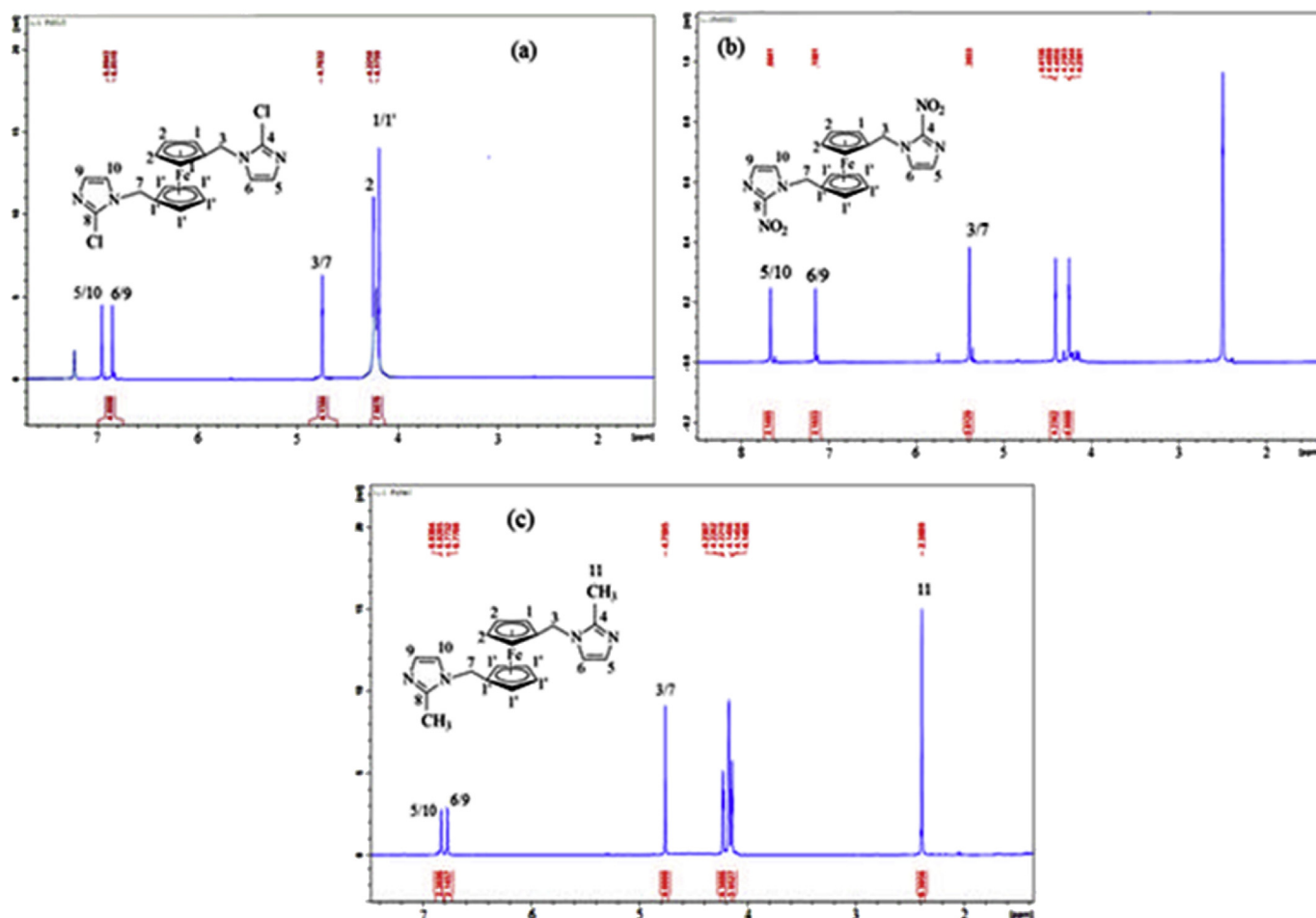
Fig. 1. ^{1}H-NMR of compounds (a) **4** (b) **5** and (c) **6**.

compound **4**, the Cp rings of the ferrocene units are slightly twisted from the ideal eclipsed conformation with C-centroid-centroid-C torsion angles of 11.46(8)°. The Cp rings in compound **4** were slightly tilted by an average angle of 2.25(3)°.

The N-C-N imidazole angles are 121.25° (N1-C13-N2) and 113.96° (N1-C7-N2) in compounds **4** and **5**, respectively; and are larger than the values for imidazole salts (107.6–108.7°) reported by Gao *et al.* [22]. This increase in bond angle could be attributed to the electron-withdrawing effect of the -Cl and -NO$_2$ substituents on the imidazole rings [38, 39]. In compound **4**, the dihedral angles between the planes of the substituted Cp rings and the imidazole ring plane are 65.58(5)°and 67.28(2)°, respectively, while in compound **5**, the dihedral angles are equal with a value of 71.46°(4). This slight change in the dihedral angle is probably due to the steric effect of the substituents on the imidazole moiety and the Cp rings [40]. The crystallographic data and structural refinement parameters for compounds **4** and **5** are shown in Table 3.

2.3. UV-visible absorption spectroscopic studies

The absorption spectra for compounds **1**–**6** are shown in Fig. 4 and the relevant absorption characteristics are given in Table 4. The spectra obtained in acetonitrile show bands at approximately 328 and 438 nm. The bands at 328 nm represent π-π* transitions from the ferrocenyl to the imidazole moiety, while the bands at 438 nm are ascribed to *d-d* transitions, probably mixed with *d-π** transitions [41]. There is a shift of the π-π* band of compounds **2** and **5**, at 328 nm bathochromically to 331 nm, attributed to the stronger electron-withdrawing effect of the nitro group on the imidazole moiety [42, 43]. This shift could also be attributed to the strong electronic communication between the enriched imidazole

and ferrocenyl moieties [44].

In order to establish the solvatochromic behaviour of compounds **1**, **3**, **4** and **6**, absorption studies were carried out in different solvents, that is, dimethylformamide (DMF) (polar aprotic), methanol (polar protic), acetonitrile (polar aprotic) and dichloromethane (DCM) (mid-polar aprotic). In all compounds, two bands (*d-d* transition and charge transfer (CT)) are observed. The data obtained are summarized in Table 5. CT transitions usually display a large solvent-dependent effect [45], resulting in negative solvatochromism as observed in methanol and DMF when compared with DCM (Fig. 5). This could be attributed to possible hydrogen-bonding between the compounds and the polar solvent molecules. It was found that the CT absorption band in compounds **1**, **3**, **4** and **6** is the same in all solvents; however, a red shift in the π-π* absorption band was observed upon a change in solvent polarity with compound **1** (showing the most significant shift from λ$_{max}$ = ~320 nm methanol/DMF to DCM) (Fig. 5). Thus, the electron-withdrawing and electron-donating substituents influenced the dipole-dipole interactions between the compounds and solvents [46]. Similar behaviour has been reported for ferrocenyl imidazole derivatives [47].

2.4. Electrochemical studies

Electrochemical studies of compounds **1**–**6** were performed in acetonitrile, with NaClO$_4$ (0.5 M) as the supporting electrolyte, at a scan rate of 100 mV/s. Fig. 6 shows the cyclic voltammograms (CV), while the corresponding electrochemical data are presented in Table 6. The CV of the substituted ferrocenyl imidazole compounds exhibit the electrochemical oxidation wave of the ferrocene/ferrocenium ion, and this is coupled with a quasi-reversible peak. Compounds **1**–**6** show one fully or
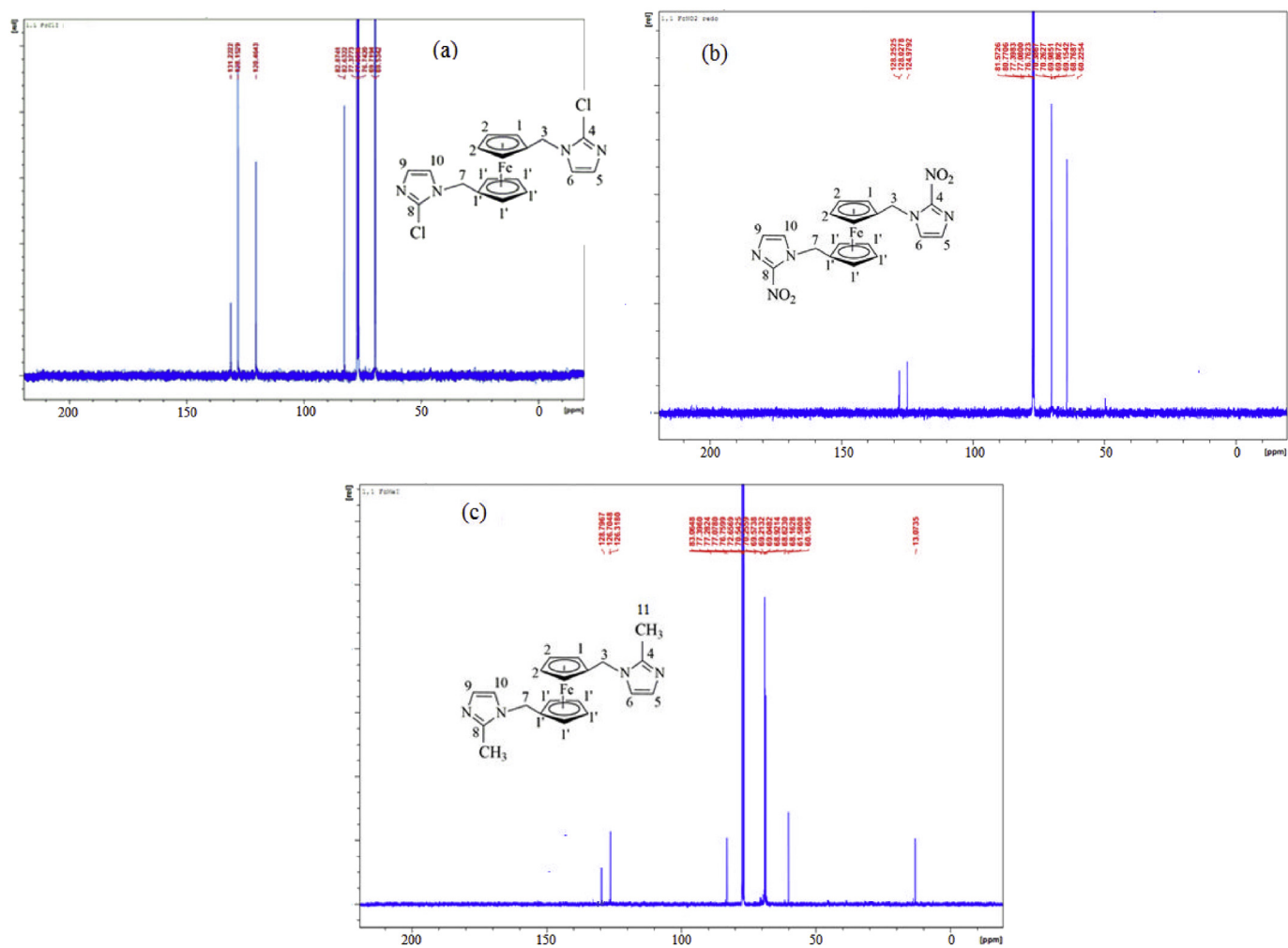
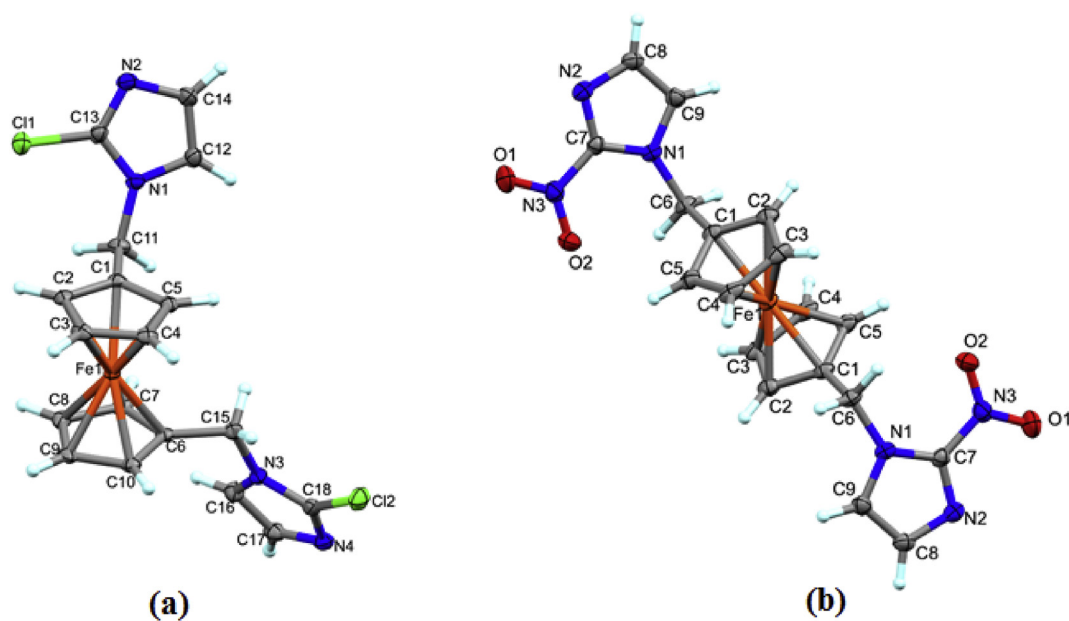Fig. 2. ^{13}C-NMR of compounds (a) 4 (b) 5 and (c) 6.

Fig. 3. *ORTEP* diagrams, along with the atom-numbering scheme for compounds (a) 4 and (b) 5. The thermal ellipsoids are depicted at 50% probability.

Table 2

Selected bond lengths (Å) and angles (°) for compounds **4** and **5**.

4		5	
C(1)-C(11)	1.503(2)	C(1)-C(6)	1.496(2)
C(11)-N(1)	1.469(8)	C(6)-N(1)	1.487(8)
N(2)-C(13)-N(1)	114.08(13)	N(1)-C(7)-N(2)	121.76(14)
N(1)-C(11)-C(1)	112.28(12)	C(7)-N(1)-C(6)	132.00(13)
C(11)-C(1)-C(6)-C(15)	79.42(1)	C(6)-C(1)-C(1)-C(6)	180
C(4)-C(5)-C(1)	108.17(13)	C(1)-C(2)-C(3)	108.13(14)
C(2)-Fe(1)	2.045(14)	C(2)-Fe(1)	2.042(6)
C(5)-Fe(1)	2.034(14)	C(5)-Fe(1)	2.036(15)

Table 3

Crystallographic data and structural refinement parameters for compounds **4** and **5**.

	4	5
Empirical formula	$C_{18}H_{16}Cl_2FeN_4$	$C_{18}H_{16}FeN_6O_4$
Formula weight	411.07	436.22
T(K)	173(2)	100(2)
λ (Å)	0.71073	0.71073
Crystal system	Monoclinic	Monoclinic
Space group	$P2_1/n$	$C2/c$
Unit cell dim. (Å/°)		
β	102.9480(10)°	102.539(2)°
a	8.5123(3)	10.9972(3)
b	15.7406(6)	7.5371(2)
c,	13.1687(5)	21.7869(7)
V(Å^3)	1719.59(11)	1762.78(9)
Z	4	4
σ (Mg/m^3)	1.588	1.644
μ(mm^{-1})	1.195	0.897
F (000)	832	896
Crystal size (mm^3)	0.326 × 0.319 × 0.272	0.220 × 0.160 × 0.080
θ range (°)	2.047 →27.461	1.915 → 28.321
Index ranges	-10 ≤ h ≤ 10	-11 ≤ h ≤ 14
	-20 ≤ k ≤ 9	-9 ≤ k ≤ 9
	-16 ≤ l ≤ 16	-29 ≤ l ≤ 26
Reflections collected	22847	8361
Independent reflections	3288	2173
Completeness to θ %/(°)	s	99.9 (25.242)
Data/restrs/para	3288/0/226	2173/0/133
GOOF on F^2	1.073	1.035
Final R indices, R_1, wR_2 [I > 2sigma(I)]	0.0289, 0.0811	0.0299, 0.0734
R indices (all data), R_1, wR_2	0.0305, 0.0824	0.0400, 0.0793
Largest diff. peak & hole	0.946 and -0.288 e.Å^{-3}	0.502 and -0.314 e.Å^{-3}
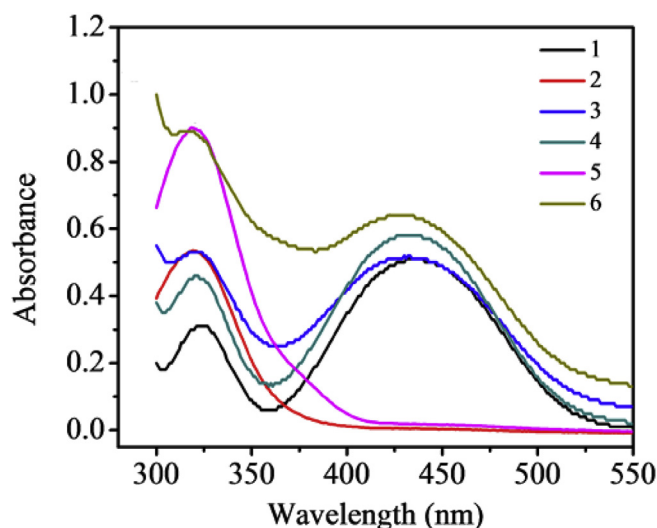
Fig. 4. UV-visible spectra of 0.005M solutions of **1**-**6** in acetonitrile.

Table 4

UV-visible absorption characteristics of compounds **1–6**.

Compounds	$λ_{max}$/nm (molar absorptivity/mol^{-1} dm^3 cm^{-1})	
	d-d	π-π*
1	438 (174)	328 (89)
2	none	331 (236)
3	438 (138)	328 (142)
4	433 (173)	328 (141)
5	none	331 (241)
6	437 (172)	328 (249)

Table 5

Absorption wavelengths of ferrocenyl imidazole derivatives in DCM, methanol, DMF and acetonitrile.

Compounds	$λ_{max}$/nm			
	DCM	Methanol	DMF	Acetonitrile
1	none	438	440	438
	343	321	320	321
2	none	none	none	none
	328	327	327	331
3	436	429	436	428
	334	320	322	321
4	446	434	442	427
	331	326	328	328
5	none	none	none	none
	329	325	327	331
6	430	427	438	438
	332	326	327	328
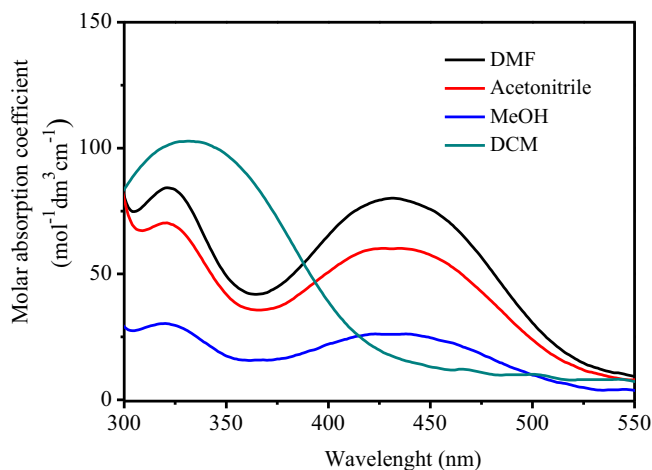
Fig. 5. UV-visible spectra of 0.005 M solutions of compound **1** in DMF, acetonitrile, methanol and DCM.

partially reversible one-electron oxidation and one or two quasi-reversible reductions for the imidazole acceptor moieties. The ferrocenyl moieties in compounds **1–6** show larger E_{pa} values than free ferrocene. The E_{pa} values follow the order: **5** > **4** > **2** > **3** > **1** > **6**, which can be related to the effect of the substituents on the redox potential of the compounds and, subsequently, the electron transfer process. Compounds **1–6** gave i_{pa}/i_{pc} ratios of approximately 1. As expected, the introduction of electron-withdrawing -Cl and -NO$_2$ substituents led to a more positive shift in the redox potential [48].

The CV curves of compounds **2** and **5** showed poorly resolved ferrocene-based waves (Fig. 6a and b). Probably the use of a coordinating solvent (i.e. acetonitrile) masked irregular features of the CV curves for compounds **2** and **5**. The two observed waves for compounds **1**, **3**, **4** and **6** are associated with the typical symmetrical dimers which produce a mixed valent transition upon reduction or oxidation. Reductions
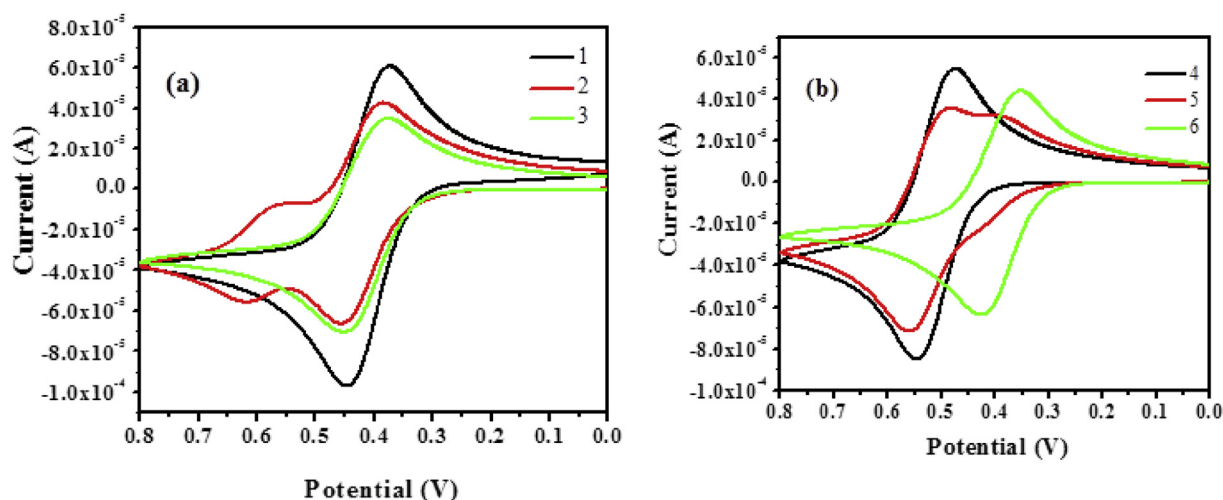
Fig. 6. Cyclic voltammogram of compounds (a) **1–3** and (b) **4–6** in 0.5 M NaClO$_4$/acetonitrile at a platinum working electrode.

Table 6
Cyclic voltammetry data for compounds **1–6**.

Compound	E$_{pa}$ (mV)	E$_{pc}$ (mV)	ΔE$_p$ (mV)	E$_{1/2}$ (mV)	i$_{pa}$/i$_{pc}$
Ferrocene [52]	470	413	57	442	1.170
1	446	373	73	410	1.129
2	456	385	71	421	1.279
3	452	376	76	414	1.168
4	546	475	71	511	1.111
5	560	484	76	522	1.014
6	426	353	73	390	1.075

E$_{pa}$, anodic oxidation potential; E$_{pc}$, cathodic reduction potential; $E_{1/2}$, redox peak potential; $(E_{1/2} = (E_{pa} + E_{pc})/2)$; ΔE$_p$ = E$_{pa}$ - E$_{pc}$.

potentials on the side groups of symmetrical complexes that generate mixed valent intermediates have been reported [49]. These systems either allow electron delocalization from direct metal-metal interaction or through the bridge path. The mixed valent intermediate group of the ferrocenyl and the ferrocenium group could be influenced by the electronegativities of the attached group.

$E_{1/2}$ of mono-substituted derivatives, compounds **1–3**, is between 410–421 mV, while the di-substituted derivatives, compounds **4–6**, displayed $E_{1/2}$ values in the range of 390–522 mV. Compound **5** has the highest $E_{1/2}$ values, thus higher reduction propensity, while compound **6** gave the lowest $E_{1/2}$ value indicating less favourable reduction of the Fe centre. From our results, compounds **2, 4** and **5** show relatively high $E_{1/2}$ values (421, 511 and 522 mV, respectively), corresponding to the oxidation of the ferrocenyl moiety, attributable to the electron-withdrawing effect of the -Cl and -NO$_2$ substituents on the imidazole moiety, compared with compounds **1, 3** and **6** [5,50,51]. The E_{pa} values for mono- and di-substituted ferrocenyl derivatives were shifted to more positive potentials (426–560 mV) compared with that of unsubstituted ferrocene (413 mV) (Table 6).

2.5. Theoretical calculation

To obtain a better insight into the electronic nature and electrochemical properties of compounds **1–6**, DFT calculations were carried out with the B3LYP functional and M06-L with def2-TZVP. The optimized geometries of compounds **4** and **5** were in good agreement with the experimental ones obtained from single crystal XRD analysis (Fig. 3).

The molecular orbitals considered were the second highest (HOMO-1) and highest (HOMO) occupied once and the lowest (LUMO) and second-lowest (LUMO+1) unoccupied ones. Fig. 7 shows the frontier molecular orbitals (HOMO and LUMO) of compound **5**. Generally, the

systems are characterized by relatively low energies for LUMO and LUMO+1 (Table 7). It is evident from Fig. 7 that, in compound **5**, the LUMO resides in the imidazole moiety while the HOMO is intense on the ferrocene ring. The high energies obtained for HOMO and HOMO-1 reflect the ability of electron donation [53]. Compound **3** has the highest HOMO and HOMO-1 values (-0.171 eV and -0.172 eV, respectively, Table 7), and this is due to the effect of the electron-donating group on the imidazole moiety, which increases the orbital energies of the ferrocenyl receptor [54]. These results indicate that more energy is involved during the electron transition in the HOMO relative to LUMO. The difference between E$_{HOMO}$ and E$_{LUMO}$ yields the band gap energy (ΔE), which is an important stability index [55]. A smaller band gap is a measure of greater prospect for transfer of electrons within a given system [56]. Compounds **2** and **5** gave the smallest band gap energies of 0.073 and 0.085 eV, respectively (Table 7). The HOMO–LUMO energy gaps of compounds **1–6** was found to approximately agree with the band gap energies calculated from the electrochemical (Table 7). As illustrated in Fig. 7, excitation from lower to lowest unoccupied orbital reflects a localized density on the functional groups while the electrons are highly occupied in the parent (ferrocene) moiety. The results obtained in Table 7 indicated that the ΔE corresponds to CT transitions in all the compounds.

3. Conclusion

Novel ferrocene derivatives, namely of compounds **4–6**, were synthesized and characterized. The single crystal X-ray crystallographic analysis of compounds **4** and **5** showed the preferred solid-state conformation and symmetry of the di-substituted ferrocenyl moiety. The electrochemical behaviour of the compounds was studied by cyclic voltammetry which shows one fully or partially reversible one-electron oxidation and one or two quasi-reversible reductions for the imidazole acceptor moieties with band gaps similar to those obtained from DFT calculations. The electron transfer process and redox behaviour of compounds **1–6** are affected by the electron-donating and withdrawing substituent on the imidazole moiety. Thus, the optical and electronic properties of the synthesized compounds can be fine-tuned by changing the substituent groups on the imidazole ring.

4. Experimental

2-Nitro-1H-imidazole (≥98.1%), 2-chloro-1H-imidazole (≥98.2%), 2-methyl-1H-imidazole (>98%), ferrocenemethanol (98%) and 1,1′-ferrocenedimethanol (98%) were supplied by Sigma Aldrich. Sodium borohydride (95%) and glacial acetic acid (99.8%) were supplied by
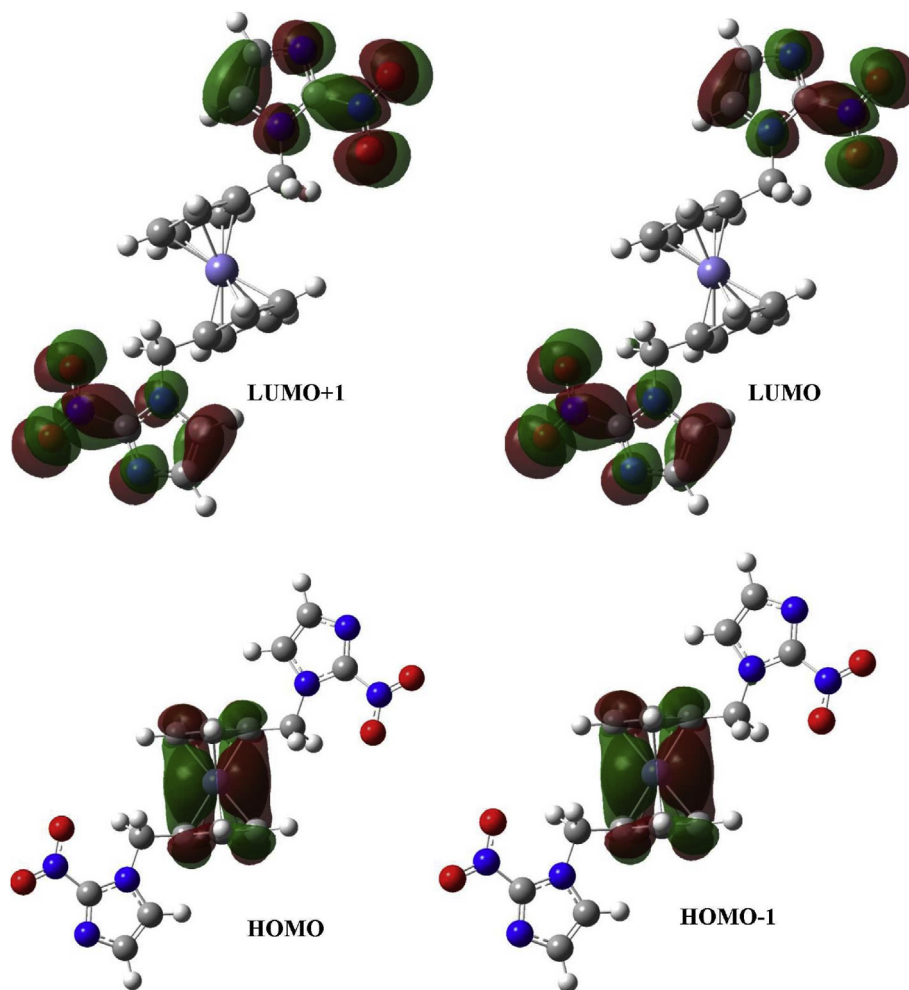
Fig. 7. Lobes of the frontier molecular orbitals for the symmetric compound **5** obtained from the M1 theoretical model.

Table 7
Frontier molecular orbital energies and quantum chemical descriptors of compounds **1**–**6** obtained from M1 level of theory.

Compound	LUMO+1 (eV)	LUMO (eV)	HOMO (eV)	HOMO-1 (eV)	ΔE^* (eV)	ΔE (CV) (eV)
1	-0.045	-0.046	-0.172	-0.173	0.127	0.073
2	-0.054	-0.107	-0.180	-0.181	0.073	0.081
3	-0.044	-0.045	-0.171	-0.172	0.126	0.070
4	-0.058	-0.058	-0.184	-0.185	0.126	0.121
5	-0.115	-0.115	-0.200	-0.200	0.085	0.070
6	-0.052	-0.053	-0.178	-0.179	0.126	0.160

* ΔE - calculated band gap energy.

Merck chemicals. All other solvents used were of analytical grade and were used as supplied by Sigma Aldrich, unless stated otherwise. TLC with varying solvent polarity was performed on silica gel 60 F_{254} plates. Silica gel with 0.063–0.2 mm mesh size was used for column chromatography to purify the products obtained. The melting point of each compound was determined using an open-end capillary tube in a Bibby Stuart Scientific model SMP3 apparatus. Infrared spectra were obtained with a PerkinElmer Spectrum 100 FTIR spectrometer fitted with a universal ATR accessory. ^{1}H-NMR and ^{13}C-NMR spectra were recorded on a 400 MHz Bruker AVANCE III spectrometer at room temperature using deuterated $CDCl_3$ or DMSO as solvents. Mass spectra of the synthesized compounds were obtained from an Agilent Technologies, 1100 series, ion-trap mass spectrometer. Electronic spectra were recorded on a

PerkinElmer Lambda 35 double-beam UV–visible spectrophotometer with 10 mm path length quartz cuvettes in acetonitrile, dichloromethane, and DMF. Cyclic voltammetry measurements were performed with a CHI660E electrochemical workstation (CH Instruments, USA) with a scan rate of 100 mV/s^{-1} in a three-electrode system consisting of a GCE (3.0 mm diameter) auxiliary electrode, Ag/AgCl reference electrode and a platinum-wire as the working electrode. The half-wave potential ($E_{1/2}$) values were obtained using (E_{pa} + E_{pc})/2, where E_{pa} and E_{pc} are the anodic and cathodic peak potentials, respectively. The band gap energies were estimated from the empirical relation E_{LUMO} = [(E_{red} - $E_{1/2}$(ferrocene)) + 4.8] eV or E_{HOMO} = [(E_{ox} - $E_{1/2}$(ferrocene)) + 4.4] eV. Ferrocene was used as an external standard. It shows two peaks at 0.38 and 0.45 V hence the $E_{1/2}$ (ferrocene) is equal to 0.42 V. The longest absorption wavelength λ_{onset} was used to calculate the optical gap energy, ΔE (Optical), according to the equation E_g = 1242/λ_{onset}.

4.1. General procedure for the synthesis of compounds 4–6

4.1.1. Representative procedure for 4–6
The prepared 1,1′-ferrocenedimethanol (240.9 mg, 1 mM) and 2-chloro-1H-imidazole (262.3 mg, 2.32 mM) in acetic acid (3 mL) were stirred for 6 hours at 60 °C. Product formation was monitored by using TLC plates with ethyl acetate/hexane (2:1) as eluent. The reaction mixture was extracted with ethyl acetate (50 mL), washed with 15 mL brine solution and dried over anhydrous sodium sulphate. Thereafter, the solvent was removed under reduced pressure to obtain the crude product which was purified by flash column chromatography on silica gel to give

a yellow solid.

4.1.2. Synthesis of 1,1′-ferrocenylmethyl(2-chloroimidazole) (4)

The general procedure described in Section 4.1.1 was followed by using 1,1′-ferrocenedimethanol (246.0 mg, 1 mM) and 2-chloro-1H-imidazole (237.8 mg, 2.20 mM). The product was purified by column chromatography and concentrated under vacuum to obtain yellow crystals as the product. Yield: 60% (245.0 mg), R_f = 3.0, m.p = 170–174 °C. IR (cm^{-1}): 439.01, 736.00, 820.00, 1036.00, 1334.37, 1465.70, 1702.04, 2923.79, 3100.43. ^{1}H-NMR spectra (400 MHz, CDCl$_3$, δ ppm): δ = 4.17–4.22 (8H, t, 2 C$_5$H$_4$), 4.76 (4H, s, 2 (CH$_2$)), 6.85 (2H, s, imidazole CH=CH), 6.89 (2H, s, imidazole CH=CH) ppm. ^{13}C-NMR spectra (400 MHz, CDCl$_3$, δ ppm): δ = 14.11, 22.67, 29.64, 30.92, 45.87, 69.53, 69.71, 76.74, 77.06, 77.38, 82.63, 120.46, 128.15, 131.22, 206.98. HR-MS (C$_{18}$H$_{16}$Cl$_2$FeN$_4$). ES: [M]$^+$ m/z calc. 414.00910, found [M + Na]$^+$ 436.9902.

4.1.3. Synthesis of 1,1′-ferrocenyl(2-nitroimidazole) (5)

The general procedure described in Section 4.1.1 was followed by using 1,1′-ferrocenedimethanol (246.0 mg, 1 mM) and 2-nitro-1H-imidazole (262.3 mg, 2.32 mM). The product was purified by column chromatography and concentrated under vacuum to obtain orange crystals. Yield: 56% (242.2 mg), R_f = 0.59, m.p = 245 °C. IR (cm^{-1}): 437.66, 831.62, 916.65, 1023.23, 1143.93, 1237.14, 1270.40, 1353.90, 1479.86, 1526.93, 1661.18, 2867.87, 3116.37, 3385.49. ^{1}H-NMR spectra (400 MHz, CDCl$_3$, δ ppm): δ = 4.23–4.25 (8H, t, 2 C$_5$H$_4$), 5.39 (4H, s, 2(CH$_2$)), 7.15 (2H, s, imidazole CH=CH), 7.66 (2H, s, imidazole CH=CH) ppm. ^{13}C-NMR spectra (400 MHz, CDCl$_3$, δ ppm): δ = 30.89, 29.62, 39.83, 40.03, 49.28, 49.66, 60.22, 68.77, 69.86,70.26, 77.08, 77.33, 80.77, 81.57, 124.97, 128.02, 207.32. HR-MS (C$_{18}$H$_{16}$FeN$_6$O$_4$). ES: [M]$^+$ m/z calc. 436.05800, found [M + Na]$^+$ 459.04801.

4.1.4. Synthesis of 1,1′-ferrocenylmethyl(2-methylimidazole) (6)

The general procedure described in Section 4.1.1 was followed by using 1,1′-ferrocenedimethanol (246.0mg, 1 mM) and 2-methyl-1H-imidazole (190.5 mg, 2.32 mM). The product was purified by column chromatography and concentrated under vacuum to obtain orange solid. Yield: 64% (239.0 mg), R_f = 2.44, m.p = 258 °C; IR (cm^{-1}): 487.66, 691.80, 831.62, 916.65, 1023.23, 1113.93, 1237.14, 1270.40, 1479.86, 1526.93, 1661.18, 2867.87, 3116.37, 3385.49. ^{1}H-NMR spectra (400 MHz, CDCl$_3$) 2.39 (6H, s, 2(CH$_3$)), 4.14–4.23 (8H, t, 2 C$_5$H$_4$), 4.76 (4H, s, 2(CH$_2$)), 6.77 (2H, s, imidazole), 6.83 (2H, s, imidazole CH=CH). ^{13}C-NMR spectra (400 MHz, CDCl$_3$): δ (ppm) = 10.96, 13.07, 14.05, 23.74, 28.92, 29.35, 30.35, 38.72, 45.42, 60.15, 61.58, 68.62, 69.04, 70.26, 72.66, 76.76, 77.07, 77.28, 89.00, 119.00, 126.32, 128.79, 130.89, 132.43, 143.93, 167.77. HR-MS (C$_{20}$H$_{22}$FeN$_4$). ES: [M]$^+$ m/z calc. 374.30012, found 374.30215.

4.2. X-ray crystal structures

Crystals of compounds **4** and **5** were attached onto the tip of a glass fibre with epoxy glue and centered in the X-ray beam under a video camera. Crystal evaluation and data were done and collected on a Bruker Smart APEX2 diffractometer with Mo Kα radiation (λ = 0.71073 Å) equipped with an Oxford Cryostream low-temperature apparatus. Omega scans of 0.5° width with an exposure time of 20 s per frame were used for data collection. The total number of images was based on results from the program COSMO [57] with the completeness of 100% out to 0.75 Å and expected redundancy was expected to be 4.0. The initial cell matrix was determined from three series of scans collected at intervals of 0.5° in a 6° range, with each of the series of scans collected at different starting angles and the APEXII [58] program suite employed for reflection indexing. Cell parameters were retrieved using APEXII [58] and refined by using SAINT [59] on all observed reflections. The structures were solved by the direct method using the SHELXS [60] program and refined. The visual crystal structures were presented using ORTEP-3 [61] and MERCURY

[62]. Non-hydrogen atoms were first refined with anisotropic displacement parameter and then by anisotropic refinement with full-matrix least squares.

Ten different DFT models (B3LYP, [63, 64] B3LYP-D2, B3LYP-D3, [65] CAM-B3LYP, [66] BMK, M05-2X, M06, M06-2X, M06-HF and M06-L [67, 68]) with def2-TZVP [69] and 6-311+G(d) [70, 71] basis sets were examined. M06-L [68] plus either basis sets proved to be sufficient and more accurate than the rest of the DFT models studied. Calculations were executed within the Gaussian 09 RevD.01 software [72] and pre/post molecular analyses were carried out in GaussView [73].

4.2.1. Crystallographic data

Crystallographic data (excluding structure factors) have been deposited with the Cambridge Crystallographic Data Centre and can be obtained free of charge *via* www.ccdc.cam.ac.uk/data_request/cif. The supplementary crystallographic data of compounds **4** and **5** are contained in CCDC 1854200 and 1854185 publication number, respectively.

Declarations

Competing interest statement

The authors declare no conflict of interest.

Additional information

No additional information is available for this paper.

References

[1] W. Yang, Z. Yin, C.-H. Wang, C. Huang, J. He, X. Zhu, J.-P. Cheng, New redox anion receptors based on calix [4] pyrrole bearing ferrocene amide, Tetrahedron 64 (2008) 9244–9252.

[2] M. Takase, M. Inouye, Ferrocene-modified bis (spiropyridopyran) s as synthetic signaling receptors for guanine–guanine dinucleoside derivatives, Chem. Commun. 23 (2001) 2432–2433.

[3] Á. Lorenzo, E. Aller, P. Molina, Iminophosphorane-based synthesis of multinuclear ferrocenyl urea, thiourea and guanidine derivatives and exploration of their anion sensing properties, Tetrahedron 65 (2009) 1397–1401.

[4] S. Quintal, T.S. Morais, C.P. Matos, M.P. Robalo, M.F.M. Piedade, M.J.V. de Brito, M.H. Garcia, M. Marques, C. Maia, L. Campino, Synthesis, structural characterization and leishmanicidal activity evaluation of ferrocenyl N-heterocyclic compounds, J. Organomet. Chem. 745 (2013) 299–311.

[5] H.-T. Niu, Z. Yin, D. Su, D. Niu, Y. Ao, J. He, J.-P. Cheng, Ferrocene-based imidazolium receptors for anions, Tetrahedron 64 (2008) 6300–6306.

[6] M. Krejčík, M. Daněk, F. Hartl, Simple construction of an infrared optically transparent thin-layer electrochemical cell: Applications to the redox reactions of ferrocene, Mn$_2$(CO)$_{10}$ and Mn(CO)$_3$(3, 5-di-t-butyl-catecholate)−, J. Electroanal. Chem. Interfacial Electrochem. 317 (1991) 179–187.

[7] C. Biot, G. Glorian, L.A. Maciejewski, J.S. Brocard, O. Domarle, G. Blampain, P. Millet, A.J. Georges, H. Abessolo, D. Dive, Synthesis and antimalarial activity in vitro and in vivo of a new ferrocene− chloroquine analogue, J. Med. Chem. 40 (1997) 3715–3718.

[8] J. Rochford, A.D. Rooney, M.T. Pryce, Redox control of meso-zinc (II) ferrocenylporphyrin based fluorescence switches, Inorg. Chem. 46 (2007) 7247–7249.

[9] Z. Wang, P. Lu, S. Chen, Z. Gao, F. Shen, W. Zhang, Y. Xu, H.S. Kwok, Y. Ma, Phenanthro [9, 10-d] imidazole as a new building block for blue light emitting materials, J. Mater. Chem. 21 (2011) 5451–5456.

[10] S. Mortazavi-Derazkola, M. Salavati-Niasari, O. Amiri, A. Abbasi, Fabrication and characterization of $Fe_3O_4@$ $SiO_2@$ $TiO_2@$ Ho nanostructures as a novel and highly efficient photocatalyst for degradation of organic pollution, J. Energy Chem. 26 (2017) 17–23.

[11] L.M. Ombaka, P.G. Ndungu, V.O. Nyamori, Tuning the nitrogen content and surface properties of nitrogen-doped carbon nanotubes synthesized using a nitrogen-containing ferrocenyl derivative and ethylbenzoate, J. Mater. Sci. 50 (2015) 1187–1200.

[12] Y. Patil, R. Misra, Tetracyanobutadiene bridged ferrocene and triphenylamine functionalized pyrazabole dimers, J. Organomet. Chem. 840 (2017) 23–29.

[13] H. Cheng, C. Ma, Y. Chen, H.L. Ni, C. Feng, B.Q. Wang, K.Q. Zhao, W.H. Yu, P. Hu, Monosubstituted ferrocene liquid crystals containing click triazole with a wide nematic phase temperature range, Liquid Crystals 44 (2017) 1450–1461.

[14] I. Manners, Synthetic Metal-Containing Polymers, John Wiley & Sons, 2006.

[15] V. Rosa, A.P. Gaspari, F. Folgosa, C.M. Cordas, P. Tavares, T. Santos-Silva, S. Barroso, T. Avilés, Imine ligands based on ferrocene: synthesis, structural and Mössbauer characterization and evaluation as chromogenic and electrochemical sensors for Hg^{2+}, New J. Chem. 42 (2018) 3334–3343.

[16] X. Zhang, L. Chen, J. Yun, J. Kong, Novel ferrocene-containing organosilicon polymers and uniform microspheres prepared by free radical copolymerization: Precursors for magnetic Si-C-Fe-(O), Mater. Design 144 (2018) 86–97.

[17] J. He, F. Guo, X. Li, W. Wu, J. Yang, J. Hua, New bithiazole-based sensitizers for efficient and stable dye-sensitized solar cells, Chem. A Eur. J. 18 (2012) 7903–7915.

[18] S. Lubov'V, A.A. Simenel, Y.S. Nekrasov, E.A. Morozova, Z.A. Starikova, S.M. Peregudova, Y.V. Kuzmenko, V.N. Babin, L.A. Ostrovskaya, N.V. Bluchterova, Synthesis, structure and redox potentials of biologically active ferrocenylalkyl azoles, J. Organomet. Chem. 689 (2004) 2473–2479.

[19] V. Boev, P. Betankourt, L. Popova, V. Babin, Alpha-ferrocenylalkylation of polyfunctional nucleophilic compounds, J. Gen. Chem USSR 61 (1991) 1516–1526.

[20] S. Lubov'V, V.I. Boev, Y.S. Nekrasov, M.M. Ilyin, V.A. Davankov, Z.A. Starikova, A.I. Yanovsky, A.F. Kolomiets, V.N. Babin, Synthesis and structure of biologically active ferrocenylalkyl polyfluoro benzimidazoles, J. Organomet. Chem. 580 (1999) 26–35.

[21] Y. Gao, B. Twamley, J.N.M. Shreeve, The first (ferrocenylmethyl) imidazolium and (ferrocenylmethyl) triazolium room temperature ionic liquids,, Inorg. Chem. 43 (2004) 3406–3412.

[22] A.A. Simenel, E.A. Morozova, Y.V. Kuzmenko, S. Lubov'V, Simple route to ferrocenyl (alkyl) imidazoles, J. Organomet. Chem. 665 (2003) 13–14.

[23] B. Bildstein, M. Malaun, H. Kopacka, K. Wurst, M. Mitterböck, K.-H. Ongania, G. Opromolla, P. Zanello, N,N'-Diferrocenyl-N-heterocyclic carbenes and their derivatives, Organometallics. 18 (1999) 4325–4336.

[24] G. Wilkinson, F.G.A. Stone, E.W. Abel, Comprehensive Organomet. Chem., Vol. 4, Pergamon Press, 1982.

[25] M. Alfonso, A. Espinosa Ferao, A. Tárraga, P. Molina, Electrochemical and fluorescent ferrocene-imidazole-based dyads as ion-pair receptors for divalent metal cations and oxoanions, Inorg. Chem. 54 (2015) 7461–7473.

[26] M. Alfonso, A. Tárraga, P. Molina, Preparation and sensing properties of a nitrogen-rich ferrocene-imidazole-quinoxaline triad decorated with pyrrole rings, Dalton Trans. 45 (2016) 19269–19276.

[27] M. Patra, G. Gasser, N. Metzler-Nolte, Small organometallic compounds as antibacterial agents, Dalton Trans. 41 (2012) 6350–6358.

[28] E.P. Çoban, R. Fırıncı, H. Biyik, M.E. Günay, Unsymmetrically substituted imidazolium salts: Synthesis, characterization and antimicrobial activity, Brazilian J. Pharm. Sci. (2017) 53.

[29] A.H. Labulo, N.P. Ngidi, B. Omondi, V.O. Nyamori, Physicochemical properties of nitrogen-doped carbon nanotubes from metallocenes and ferrocenyl imidazolium compounds, J. Organomet. Chem. 868 (2018) 66–75.

[30] M. Salavati-Niasari, Z. Behfard, O. Amiri, E. Khosravifard, S.M. Hosseinpour-Mashkani, Hydrothermal synthesis of bismuth sulfide (Bi_2S_3) nanorods: Bismuth (III) monosalicylate precursor in the presence of thioglycolic acid, J. Cluster Sci. 24 (2013) 349–363.

[31] E. Fleming, F. Du, E. Ou, L. Dai, L. Shi, Thermal conductivity of carbon nanotubes grown by catalyst-free chemical vapor deposition in nanopores, Carbon 145 (2019) 195–200.

[32] Y. Wei, Z. Yang, G. Zhao, W. Yang, Synthesis and catalytic properties of macroporous SiO_2-coated CNT-sieve-composite-supported 12-tungstophosphoric acid catalysts with dual pore structure for the Baeyer–Villiger oxidation of cyclic ketones under microwave irradiation, J. Catal. 371 (2019) 196–206.

[33] A.N. Nasir, N. Yahaya, N.N. Zain, V. Lim, S. Kamaruzaman, B. Saad, N. Nishiyama, N. Yoshida, Y. Hirota, Thiol-functionalized magnetic carbon nanotubes for magnetic micro-solid phase extraction of sulfonamide antibiotics from milks and commercial chicken meat products, Food Chem. 276 (2019) 458–466.

[34] P. He, Y. Du, S. Wang, C. Cao, X. Wang, G. Pang, Y. Shi, Synthesis, structure, and reactivity of ferrocenyl-NHC palladium complexes, Z. Anorg. Allg. Chem. 639 (2013) 1004–1010.

[35] V.O. Nyamori, M. Gumede, M.D. Bala, Synthesis, characterisation and properties of ferrocenylalkylimidazolium salts, J. Organomet. Chem. 695 (2010) 1126–1132.

[36] A.W. Taylor, P. Licence, X-ray photoelectron spectroscopy of ferrocenyl-and ferrocenium-based ionic liquids, ChemPhysChem 13 (2012) 1917–1926.

[37] P. Kübler, J. Sundermeyer, Ferrocenyl-phosphonium ionic liquids–synthesis, characterisation and electrochemistry, Dalton Trans. 43 (2014) 3750–3766.

[38] J.-F.O. Longeval, A. Langlois, A. Buisson, C.H. Devillers, S.B. Clément, A. Van Der Lee, P.D. Harvey, S.B. Richeter, Synthesis, characterization, and electronic properties of porphyrins conjugated with N-heterocyclic carbene (NHC)–gold (I) complexes, Organometallics 35 (2016) 663–672.

[39] R. Balasubramanian, W. Wang, R.W. Murray, Redox ionic liquid phases: Ferrocenated imidazoliums, J. Am. Chem. Soc. 128 (2006) 9994–9995.

[40] K.S. Coleman, S. Turberville, S.I. Pascu, M.L. Green, Synthesis of a new bidentate ferrocenyl N-heterocyclic carbene ligand precursor and the palladium (II) complex trans-[PdCl2 (C∧ fc∧ C)], where (C∧ fc∧ C)= 1, 1'-di-tert-butyl-3, 3'-(1, 1'-dimethyleneferrocenyl)-diimidazol-2-ylidene, J. Organomet. Chem. 690 (2005) 653–658.

[41] K. Kowalski, Ł. Szczupak, J. Skiba, O.S. Abdel-Rahman, R.F. Winter, R. Czerwieniec, B. Therrien, Synthesis, structure, and spectroelectrochemistry of ferrocenyl–meldrum's acid donor–acceptor systems, Organometallics 33 (2014) 4697–4705.

[42] Q. Zhang, W.-L. Song, A.S. Hossain, Z.-D. Liu, G.-J. Hu, Y.-P. Tian, J.-Y. Wu, B.-K. Jin, H.-P. Zhou, J.-X. Yang, Synthesis, crystal structure, electrochemistry and in situ FTIR spectroelectrochemistry of a bisferrocene pyrazole derivative, Dalton Trans. 40 (2011) 3510–3516.

[43] B. López-Mayorga, C. Sandoval-Chávez, P. Carreón-Castro, V. Ugalde-Saldívar, F. Cortés-Guzmán, J. López-Cortés, M. Ortega-Alfaro, Ferrocene amphiphilic D–π–A dyes: synthesis, redox behavior and determination of band gaps, New J. Chem. 42 (2018) 6101–6113.

[44] B. Gélinas, J.C. Forgie, D. Rochefort, Conductivity and electrochemistry of ferrocenyl-imidazolium redox ionic liquids with different alkyl chain lengths, J. Electrochem. Soc. 161 (2014) 161–165.

[45] J.E. Reid, C.E. Bernardes, F. Agapito, F. Martins, S. Shimizu, M.E.M. da Piedade, A.J. Walker, Structure–property relationships in protic ionic liquids: a study of solvent–solvent and solvent–solute interactions, Phys. Chem. Chem. Phys. 19 (2017) 28133–28138.

[46] B. Dereka, E. Vauthey, Solute–solvent interactions and excited-state symmetry breaking: Beyond the dipole–dipole and the hydrogen-bond interactions, J. Phys. Chem. Lett. 8 (2017) 3927–3932.

[47] J.-B. Zhuo, X.-X. Zhu, C.-X. Lin, S. Bai, L.-L. Xie, Y.-F. Yuan, Design, synthesis and anion recognition of ferrocene-based benzimidazolium receptors, J. Organomet. Chem. 770 (2014) 85–93.

[48] H.A. Özbek, P.S. Aktaş, J.-C. Daran, M. Oskay, F. Demirhan, B. Çetinkaya, Synthesis, structure, electrochemical and antimicrobial properties of N, N'-bis (ferrocenylmethyl) imidazolinium salts, Inorg. Chim. Acta 423 (2014) 435–442.

[49] W.C. Du Plessis, J.J.C. Erasmus, G.J. Lamprecht, J. Conradie, T.S. Cameron, M.A.S. Aquino, J.C. Swarts, Cyclic voltammetry of ferrocene-containing β-diketones as a tool to obtain group electronegativities. The structure of 3-ferrocenoyl-1, 1, 1-trifluoro-2-hydroxyprop-2-ene, Can. J. Chem. 77 (1999) 378.

[50] G. Zhou, M. Baumgarten, K. Müllen, Arylamine-substituted oligo (ladder-type pentaphenylene) s: Electronic communication between bridged redox centers, J. Am. Chem. Soc. 129 (2007) 12211–12221.

[51] Y. Shi, L. Xiao, D. Wu, F. Li, D. Li, J. Zhang, S. Li, H. Zhou, J. Wu, Y. Tian, Synthesis, crystal structure, electrochemistry and third-order nonlinear optical properties of two novel ferrocene derivatives, J. Organomet. Chem. 817 (2016) 36–42.

[52] E.M. Njogu, B. Omondi, V.O. Nyamori, Synthesis, physical and antimicrobial studies of ferrocenyl-N-(pyridinylmethylene) anilines and ferrocenyl-N-(pyridinylmethyl) anilines, S. Afr. J. Chem. 69 (2016) 51–66.

[53] C.P. Okoli, Q.J. Guo, G.O. Adewuyi, Application of quantum descriptors for predicting adsorption performance of starch and cyclodextrin adsorbents, Carbohydr. Polym. 101 (2014) 40–49.

[54] R. Manivannan, K.P. Elango, Spectral and electrochemical studies on anion recognition by ferrocene based imidazoles possessing different electron acceptor moieties, J. Organomet. Chem. 799 (2015) 99–107.

[55] A. Satheshkumar, R. Manivannan, K.P. Elango, Spectroscopic, electrochemical and theoretical studies on anion recognition by receptors with redox active ferrocene and quinone centers bridged by imidazole, J. Organomet. Chem. 750 (2014) 98–106.

[56] P. Deglmann, A. Schafer, C. Lennartz, Application of quantum calculations in the chemical industry—An overview, Int. J. Quantum Chem. 115 (2015) 107–136.

[57] Bruker, in: COSMO, Bruker AXS, Madison, WI, 2009.

[58] Bruker, in: APEXII, Bruker AXS, Madison, WI, 2009.

[59] Bruker, in: SAINT, Bruker AXS, Madison, WI, USA, 2009.

[60] G.M. Sheldrick, A short history of SHELX, Acta. Crystallogr. Sect. A 64 (2008) 112.

[61] L.J. Farrugia, WinGX and ORTEP for Windows: an update, J. Appl. Crystallogr. 45 (2012) 849.

[62] C.F. Macrae, I.J. Bruno, J.A. Chisholm, P.R. Edgington, P. McCabe, e. Pidcock, L. Rodriguez-Monge, R. Taylor, J. van de Streek, P.A. Wood. Mercury CSD 2.0–new features for the visualization and investigation of crystal structures, J. Appl. Crystallogr. 41 (2008) 466.

[63] C. Lee, W. Yang, R.G. Parr, Development of the Colle-Salvetti correlation-energy formula into a functional of the electron density, Phys Rev B. 37 (1988) 785.

[64] A.D. Becke, A new mixing of Hartree–Fock and local density-functional theories,, J. Chem. Phys. 98 (1993) 1372–1377.

[65] S. Grimme, J. Antony, S. Ehrlich, H. Krieg, A consistent and accurate ab initio parametrization of density functional dispersion correction (DFT-D) for the 94 elements H-Pu,, J. Chem. Phys. 132 (15) (2010).

[66] T. Yanai, D.P. Tew, N.C. Handy, A new hybrid exchange–correlation functional using the Coulomb-attenuating method (CAM-B3LYP),, Chem Phys Lett. 393 (2004) 51–57.

[67] Y. Zhao, N. González-García, D.G. Truhlar, Benchmark database of barrier heights for heavy atom transfer, nucleophilic substitution, association, and unimolecular reactions and its use to test theoretical methods, J Phys. Chem. A. 109 (2005) 2012–2018.

[68] Y. Zhao, D.G. Truhlar, Density functionals with broad applicability in chemistry, Acc. Chem. Res. 41 (2008) 157–167.

[69] F. Weigend, R. Ahlrichs, Balanced basis sets of split valence, triple zeta valence and quadruple zeta valence quality for H to Rn: Design and assessment of accuracy, Phys Chem Chem Phys. 7 (2005) 3297–3305.

[70] R.B. Krishnan, J.S. Binkley, R. Seeger, J.A Pople, Self consistent molecular orbital methods. XX. A basis set for correlated wave functions, J. Chem. Phys. 72 (1980) 650–654.

[71] R. McWeeny, The density matrix in self-consistent field theory. II. Applications in the molecular orbital theory of conjugated systems, in: Proceedings of the Royal Society of London A: Mathematical, Physical and Engineering Sciences, The Royal Society, 1956.

[72] M.J. Frisch, G.W. Trucks, H.B. Schlegel, G.E. Scuseria, M.A. Robb, J.R. Cheeseman, G. Scalmani, V. Barone, B. Mennucci, G.A. Petersson, H. Nakatsuji, Gaussian 09, revision D. 01, Gaussian, Inc., Wallingford CT, 2009.

[73] R. Dennington, T. Keith, J. Millam, In GaussView, Semichem Inc., Shawnee Mission KS, 2009.